Dyes and Pigments 202 (2022) 110308

Contents lists available at ScienceDirect

Dyes and Pigments

journal homepage: www.elsevier.com/locate/dyepig

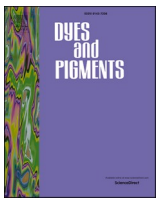

How to achieve near unity fluorescence quantum yields on gold(I) benzothiadiazole-based derivatives

Andrea Pinto [a,b], Marcelo Echeverri [c], Berta Gómez-Lor [c,**], Laura Rodríguez [a,b,*]

[a] Departament de Química Inorgànica i Orgànica, Secció de Química Inorgànica, Universitat de Barcelona, Martí i Franquès 1-11, E-08028 Barcelona, Spain
[b] Institut de Nanociència i Nanotecnologia (IN^{2}UB). Universitat de Barcelona, 08028, Barcelona, Spain
[c] Instituto de Ciencia de Materiales de Madrid, CSIC Cantoblanco, 28049, Madrid, Spain

ARTICLE INFO

Keywords:
BTD
gold(I)
Organic matrixes
Luminescence
Quantum yields

ABSTRACT

The synthesis of three new gold(I) benzothiadiazole derivatives has been carried out by the reaction of 4-ethynyl-7-(4-nonylphenyl)benzo[c] [1,2,5]thiadiazole (**L**) with three different gold(I)-PR_3 (PR_3 = triethylphosphane (**2**), triphenylphosphane (**3**) and tri-1-naphthylphosphane (**4**)) sources and their light emitting properties thoroughly investigated.

The new compounds display denoted luminescence properties with fluorescence quantum yields above 80% in all cases except for the complex containing the bulkiest $PNaph_3$ phosphane. The resulting emission is mainly dominated by the organic 2,1,3-benzothiadiazole moiety (BTD) and can be modulated following different strategies. On one hand, the emission wavelength of these compounds in solution can be *ca.* 60 nm shifted varying the polarity of the solvents. Interestingly, quantum yields and lifetimes can be strongly increased by changing the environment conditions, from water:acetonitrile solutions to dispersion of the compounds within organic matrixes. In this way, we have been able to obtain near unity fluorescence quantum yields, with the highest values recorded for gold(I) BTD compounds. The effect of the solvents on the emission changes has been rationalized with the help of the Lippert-Mataga equation and the multiparametric Kamlet-Taft method to analyse the excited state polarity.

1. Introduction

2,1,3-Benzothiadiazole (BTD) is an electron deficient heterocycle with increasing interest in the last years and that has been widely applied as a building block or dopant in the synthesis of optoelectronic compounds for a wide range of applications such as production of luminescent compounds, organic light emitting diodes (OLEDs) [1,2], organic field effect transistors (OFETs) [3], solar-hydrogen conversion [4], bioprobes [5], dye-sensitized solar cells [6] and wavelength shifting materials [7,8] among others. This moiety can be successfully functionalized in 4 and 7 positions via coupling reactions (Sonogashira, Suzuki, and Buchwald-Hartwig) giving rise to a library of different symmetrical and unsymmetrical derivatives that display interesting optical properties such as high molar extinction coefficients, large Stokes shifts, high quantum yields, high storage stability, high signal-to-noise ratios and stimuli responsive behaviour [9,10].

On the other hand, organometallic π-conjugated materials have emerged as a frontier research field over the past few decades, owing to their similar applications regarding their emissive properties. Among them, discrete molecules containing metal-alkynyl moieties and polymers arouse much attention as they favour strong interactions between the metal d-orbitals and the π-system of the ligand mediated via the metal-acetylide linkage [11]. This makes the design and development of rigid-rod metal-acetylide organometallic scaffolds for smart applications in the field of optoelectronics a rapidly growing area [12]. Gold(I) atom is well-known to coordinate to alkynyl groups of chromophores in order to obtain linear π-conjugated organometallic complexes. They are thus very attractive and promising candidates for the construction of molecular linear structures, which may possess unique luminescent properties such as long lived phosphorescence, liquid-crystallinity, and nonlinear optical behaviour, allowing their application also in electronic devices [13,14]. Furthermore, the presence of the Au(I) heavy atom and

* Corresponding author. Departament de Química Inorgànica i Orgànica, Secció de Química Inorgànica, Universitat de Barcelona, Martí i Franquès 1-11, E-08028 Barcelona, Spain.
** Corresponding author.
E-mail addresses: bgl@icmm.csic.es (B. Gómez-Lor), laura.rodriguez@qi.ub.es (L. Rodríguez).

https://doi.org/10.1016/j.dyepig.2022.110308
Received 7 February 2022; Received in revised form 31 March 2022; Accepted 1 April 2022
Available online 12 April 2022

the possibility to establish Au(I)···Au(I) weak interactions play an important role in the resulting photophysical properties and may affect the luminescence quantum yields, lifetimes, population of the triplet state and the possible formation of intermolecular aggregates [15]. The emission of these aggregated structures may be enhanced (aggregation induced emission, AIE) or quenched (aggregation caused quenching effect, ACQ) [16].

BTDs have been scarcely explored regarding AIE phenomenon [17]. The first strategy employed to develop AIE-active BTD derivatives was related to the coordination of the BTD chromophore to the well-known AIEgenic compound tetraphenylethylene (TPE) producing a green emissive film with a very high fluorescence quantum yield (φ_{Fl}) value of 0.89 [18]. The same group described also a BTD-tiophene-TPE derivative possessing three TPE units [19]. Nevertheless, to the best our knowledge, there is no precedent in the literature on the use of gold(I) BTD-AIEgenic structures. This is the strategy that will be developed in this work. In fact, the presence of heavy atoms has been extensively explored in the formation of phosphorescent compounds due to the heavy atom effect. However, in recent years, there are increasing number of reports on transition-metal complexes containing aromatic chromophores (such as perylene, perylene diimide, pyrene and tetracene) where the observed emission is ligand-dominated fluorescence and display slow ISC rate with lifetimes ranging from hundreds of ps to ns [3]. This indicates that the presence of heavy elements does not guarantee fast ISC rate and/or efficient phosphorescence emission.

Thus, in this work we will develop gold(I) AIE emitters containing BTD fluorophores. It has been reported the AIE behaviour of BTD organic compounds containing diphenylamine and triphenylamine donor ligands [20]. Analogous phosphane ligands, instead of amine, have been chosen in this work due to their stronger coordination to the gold(I) atom. It must be also considered that the ancillary phosphane ligands have been used to prevent the infinite aggregation and confine the metal surrounding to the certain size and shape [21]. Taking all of this into consideration, three different phosphanes that differ in their bulkiness have been chosen to evaluate their effect on the potential AIE emission.

2. Results and discussion

2.1. Synthesis and characterization

The synthesis of the ligand 4-ethynyl-7-(4-nonylphenyl)benzo[c] [1,2,5]thiadiazole **L** was performed starting from previously reported 4-bromo-7-(4-nonylphenyl)benzo[c] [1,2,5]thiadiazole [22] by Sonogashira coupling with ethynyl trimethylsilane, followed by deprotection with KF.

The synthesis of gold(I) complexes was performed in two different steps. A suspension of the previous synthesized BTD ethynyl derivative **L**, was firstly reacted with AuCl(tht) to yield the [Au(4-ethynyl-7-(4-nonylphenyl)benzo[c] [1,2,5]thiadiazole)]$_n$ (**1**) polymer. After isolation from the reaction medium, this polymer was reacted with one equivalent of the corresponding phosphane, PR_3, to afford the desired products [Au(4-ethynyl-7-(4-nonylphenyl)benzo[c] [1,2,5]thiadiazole)(PR_3)] (PR_3 = triethylphosphane (**2**), triphenylphosphane (**3**) and tri-1-naphthylphosphane (**4**)) in moderate-high yields, above 70% (Scheme 1).

All complexes were characterized by ^{1}H and ^{31}P NMR and IR spectroscopies and mass spectrometry. ^{1}H NMR spectra of the compounds display all corresponding protons of the aromatic rings and long alkyl chain corresponding to **L** as well as the protons related to the phosphane. The disappearance of the terminal C≡C–*H* alkynyl proton of **L** is a clear indication of the formation of the complexes. ^{31}P{^{1}H} NMR spectra display in all cases only one peak, that is *ca.* 50 ppm downfield shifted with respect to the free phosphane upon coordination to the metal atom, as previously observed in this type of syntheses (see SI) [23–26]. The characteristic vibration of υ(C≡C) around 2100 cm^{-1} is 100 cm^{-1} shifted to longer wavenumbers with respect to the polymer (**1**), as previously observed in other gold(I) alkynyl derivatives [23–26]. Mass spectra was a definitive evidence of the correct formation of the complexes and display the molecular peak $[M + H]^+$ in all cases.

2.2. X-ray crystal structure determination

Single crystals suitable for X-ray diffraction were successfully grown from dichloromethane/hexane solutions of the complexes **3** and **4**. They crystalize in the P-1 space group of the triclinic system. Selected bond length and angles are summarized in Table 1 and details of data collection and refinement in Table S1.

The crystal structure of **3** consists of two molecules in the asymmetric unit in parallel disposition but shifted with C–H···π(C≡C) weak contacts. In contrast, the unit cell of **4** contains only one molecule (Fig. 1). A linear geometry is observed for both complexes around the metal atom with a P–Au–C angle of 176°. The P–Au and Au–C distances are in agreement with those of previously reported Au(I)-acetylide complexes [23,27–35]. The torsion angles between the two aromatic rings (Table 1) decrease with the increase of the bulkiness of the phosphane that is coordinated to the gold(I) atom probably due to steric hindrance effects (see Fig. 2).

Both complexes display intermolecular C–H···N and C–H···π short

Table 1
Selected bond lengths (Å) and angles (deg) for **3** and **4**.

Compound	Distance (Å)	Angle (°)
3	Au–P: 2.275(2)	C–Au–P: 176.66(2)
	Au–C1: 1.996(6)	Torsion: 39.74(1)
	Au···Au: 9.286(6)	
4	Au–P: 2.282(1)	C–Au–P: 175.92(2)
	Au–C1: 2.018(5)	Torsion: 20.96(1)
	Au ··Au: 13.704(6)	

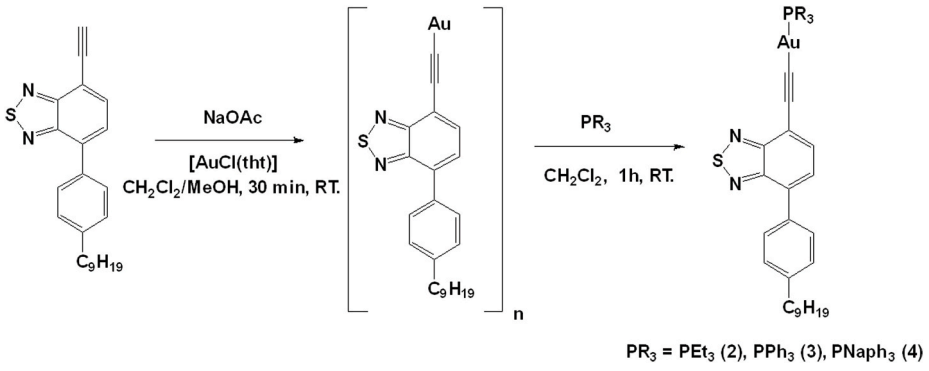

Scheme 1. Synthesis of gold(I) benzothiadiazole-based derivatives.

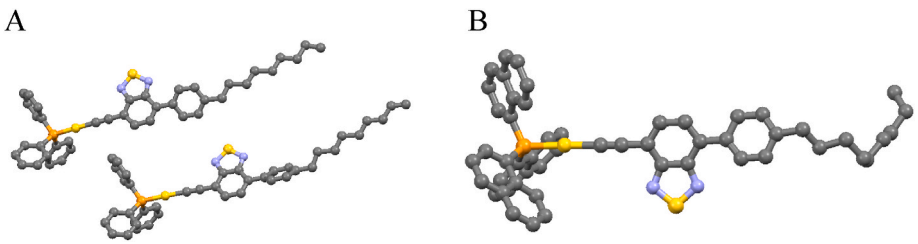

Fig. 1. Representation of the independent molecules per unit cell of **3** (A) and **4** (B). Hydrogen atoms are omitted for clarity.

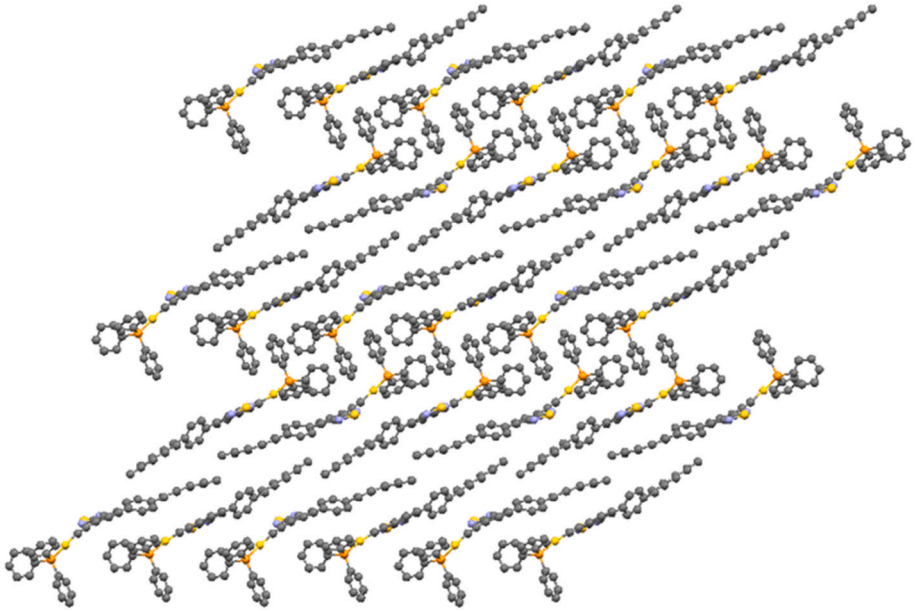

Fig. 2. Representation of the packing of **3.**

contacts in the 3D crystal packing. The packing arrangement in **3** shows an alignment of the molecules due to the presence of an aliphatic chain and additional and S···H short contacts. In the case of **4**, the aliphatic chain is twisted at the end and the molecules are aligned due to the π-π stacking of the naphthyl rings (Figs. 2 and 3 and S12-S13). The difference in the resulting packing may be due to the steric hindrance of the phosphane in **4** that precludes a linear well-ordered arrangement of the molecules. No aurophilic contacts are observed in the packing with Au···Au distances of 9.286 Å and 13.704 for **3** and **4** respectively.

2.3. Photophysical characterization

The absorption and emission spectra of all gold(I) complexes **2**–**4** and **L** precursor were recorded in 10^{-5} M dichloromethane solutions and in the solid state at room temperature and the obtained data are summarized in Table 2.

The absorption spectra of all the compounds display two absorption bands: one at higher energies related to the π→π* transition of the BTD aromatic rings and another at lower energies assigned to charge transfer (CT) transition [10,11,36] [–] [42] (Fig. 3) that is 25 nm red shifted in gold(I) complexes **2–4** when compared to that of the ligand **L**. This shift is probably ascribed to an increase in the conjugation through mixing the metal d-orbital with the π-system of the ligand [43]. Absorption spectra recorded at different concentrations (under spectroscopically concentration conditions) point out that the molecules do not aggregate in solution since a linear correlation is recorded between the absorption maxima against concentration (Figs. S14–S17). Small deviation is only recorded in the case of **4** at the highest concentration but it is above the spectroscopic conditions for this very high emissive species.

Emission spectra were recorded in solution and in solid state upon excitation of the samples at the lowest energy absorption band and it is observed that the emission of the complexes is *ca.* 20–30 nm red shifted with respect to the recorded emission of **L** (Fig. 4). The observed large Stokes shifts (around 100 nm) are a consequence of the efficient intramolecular charge transfer (ICT) [44]. The emission maxima do not change too much between solid state and solution. Excitation spectra collected at the emission maxima match the CT absorption bands at ca. 400 nm as an additional indication of their emission origin and the

Table 2
Electronic absorption and emission data, quantum yields (%) (Φ_{fl}), lifetime (τ_{fl}), k_r and k_{nr} of **L** and complexes **2–4** in dichloromethane. Bold numbers: Emission data, quantum yields, lifetimes, k_r and k_{nr} in the solid state.

Compound	Absorption spectra (CH_2Cl_2) λ_{max} ($\varepsilon \cdot 10^{-3}$, cm^{-1} M^{-1})	Emission max	Stokes shift (cm^{-1})	Φ_{fl}	τ_{fl} (ns)	k_r (μs^{-1})	k_{nr} (μs^{-1})
L	270 (20.9), 384 (10.5)	492/**485**	5716	83/**36**	9.40/**5.8**	88/**62**	18/**110**
2	287 (18.5), 409 (9.1)	519/**517**	5182	86/**6**	9.87/**3.92**	87/**14**	14/**241**
3	293 (8.0), 410 (3.8)	509/**514**	4744	87/**24**	9.19/**2.01**	94/**119**	14/**378**
4	300 (21.9), 409 (7.6)	519/**517**	5182	62/**18**	6.45/**3.78**	96/**47**	59/**217**

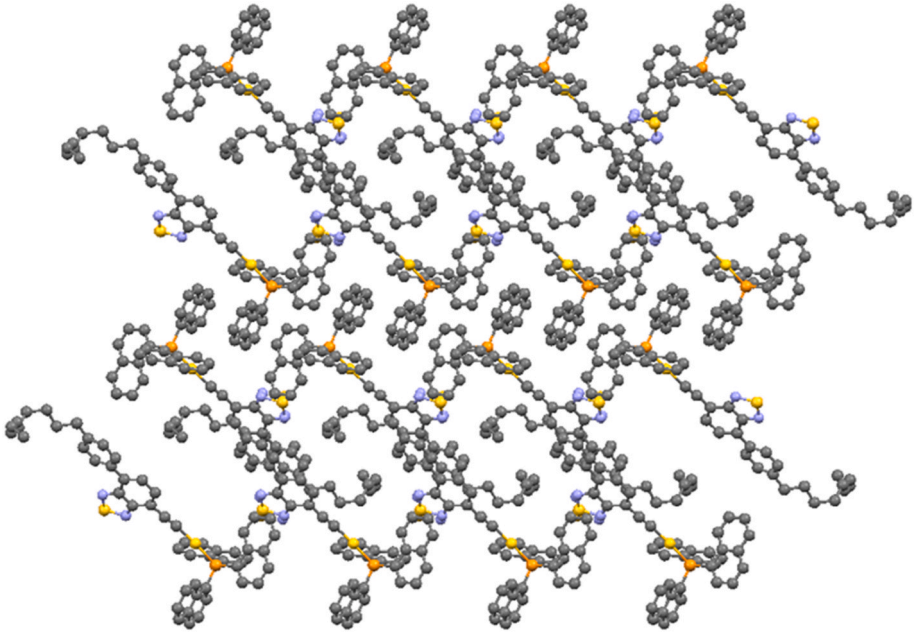

Fig. 3. Representation of the packing of **4**.

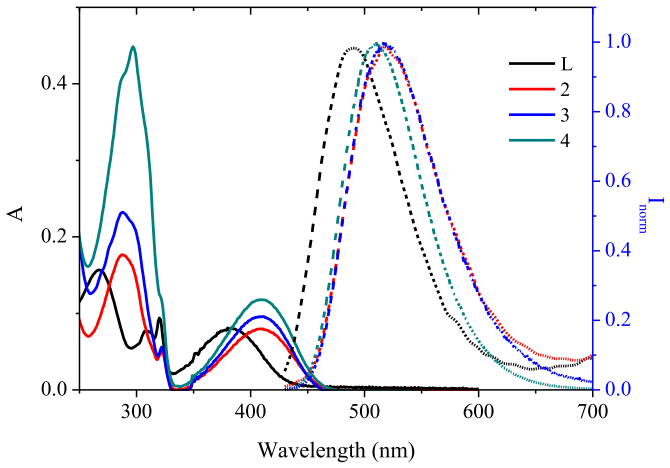

Fig. 4. Absorption (solid lines) and emission (dash lines) spectra of **L** and gold (I) complexes **2–4** in dichloromethane.

purity of the samples (Fig. S18) (see Fig. 5).

Fluorescence quantum yields (Φ_{fl}) and lifetimes (τ_{fl}) were measured in dichloromethane and in solid state for all compounds (Table 2). In general, Φ_{fl} and τ_{fl} in solution are in the same order than other BTD derivatives previously reported in the literature [5,11,17,45–47]. The recorded Φ_{fl} values are very high, between 80 and 90% (slightly higher for gold(I) complexes **2** and **3** with respect to **L**) except in the case of the gold complex **4**, substituted with the bulkiest phosphane, which displays a quantum yield, around 60% (Table 2). These values decrease significantly in the solid state (due to an aggregation caused quenching, ACQ, due to the presence of intermolecular contacts) as previously reported in the literature for other BTD derivatives [10,47]. The observed decrease is more affected for gold(I) complexes with respect to **L**. Thus, the presence of gold(I) atoms may be directly involved in the packing in the solid state probably due to the closer contact of the Au(I) atoms to the BTD chromophore in the solid that may favour intersystem crossing and population of non-emissive triplet states. Particularly lower is the quantum yield recorded for **2**, containing the less bulky phosphane and thus, with higher probabilities to perform intermolecular contacts.

The fluorescence lifetimes show a single-exponential decay with values around 9 ns in the case of **L**, **2** and **3** and 6 ns in the case of **4** (Figs. S19–S22) [10,11,47]. The calculation of the k_r and k_{nr} values from Φ_{fl} and τ_{fl} indicates that the radiative deactivation remains similar in solution, being slightly higher when increasing the bulkiness of the phosphine (complexes **3** and **4**, Table 2). More important is the effect on the non-radiative pathways of **4** with a 4-fold larger value of k_{nr} in solution, which is substituted with the bulkier phosphane, being probably the reason of the lowest fluorescence quantum yield. The effect of the heavy atom is clearly reflected in the solid state where radiative emission is in general less favored (mainly for **2** and **3** that are more suitable to establish intermolecular contacts). In contrast, the non-radiative deactivation pathways are clearly enhanced for the gold(I) complexes with k_{nr} values that are clearly larger with respect to **L**. Hence, the presence of a heavy atom is favoring alternative non-radiative processes that may be S1→ S0 internal conversion or population of non-emissive triplet state, S1→ T1.

Emission spectra were also recorded at low temperature and in deoxygenated samples (N_2-saturated solutions) in an attempt to detect possible phosphorescence emission due to the presence of the gold(I) heavy atom [48]. No phosphorescence was recorded in any case, which however does not preclude the possibility of a populated triplet state in the complexes, as stated above in the analysis of the non-radiative rate constants. Note that nanosecond-Transient Absorption (ns-TA) experiments performed on analogous complexes evidence the population of the triplet state in the presence of the gold(I) heavy atom in spite of the lack of phosphorescence [11]. Hence, this is one of the cases where intraligand fluorescence dominates the resulting emission of the complexes [3].

2.4. TD-DFT theoretical studies

Computational analysis was performed aiming at understanding the charge transfer character of the synthesized complexes. The minimum energy optimized geometries of the four compounds in the ground state together with their frontier orbitals were calculated in vacuum (Figs. 5 and S54 and Table S5). The torsion angle between the two aromatic rings have been calculated for the minimum energy optimized geometries (see Table S6). A decrease is observed with the increase on the bulkiness of phosphane ancillary ligand probably due to steric hindrance

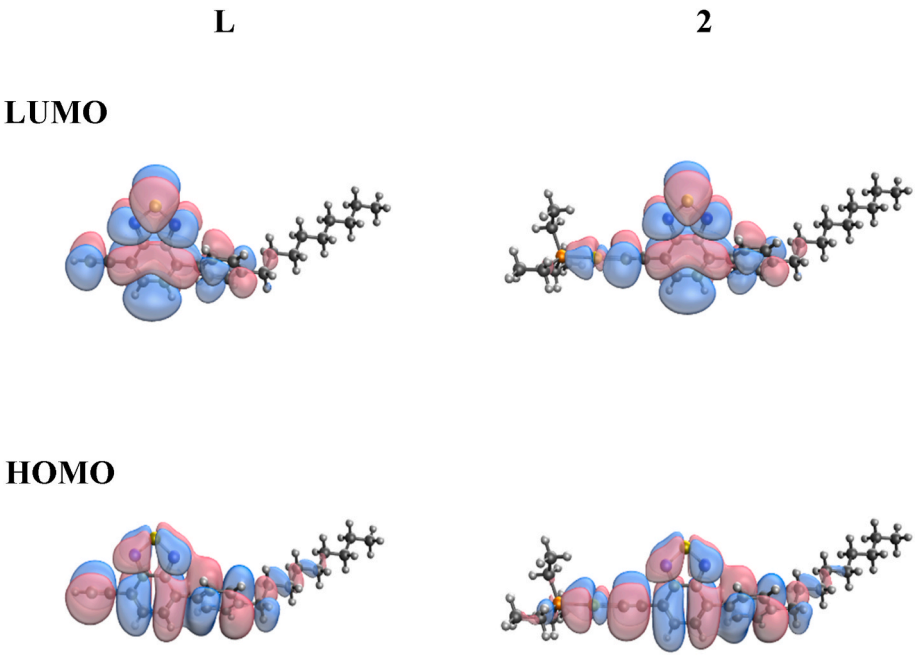

Fig. 5. Calculated HOMO and LUMO orbital densities for **L** and **2** compounds.

effects that restricts the torsion rotation. All the molecules have HOMO orbitals widely distributed across the backbone while LUMO orbitals are much more localized on the electron-acceptor benzothiadiazole unit as observed in other BTD derivatives [49]. Although the transition is mainly on the organic counterpart, the involvement of gold(I) orbitals both in the HOMO and LUMO orbitals induces a decrease on the HOMO-LUMO gap thus explaining the red-shifting observed in the UV–vis spectra of the complexes.

2.5. Electrochemical characterization

The redox properties of **L** and the gold(I) complexes **2–4** were investigated by cyclic voltammetry (CV) in CH_2Cl_2 solution (10^{-3} M) containing 0.1 M tetra-n-butylammonium hexafluorophosphate ($TBAPF_6$) as supporting electrolyte at a scan rate 100 mV/s.

All compounds show a reversible reduction process at −1.29 V for **L** and −1.38 V for gold(I) complexes **2–4** (Fig. 6). The reduction potential moves to more negative values when $Au(PR_3)$ is coordinated to the alkynyl moiety. This is indicative of an increase of the electron density in the π system [36] due to the coordination of the gold(I) in the chemical structure as previously seen in similar compounds containing alkynyl-gold(I)-PR_3 moieties [60]. Compounds **2–4** show also an irreversible oxidation process at 1.38 V .

The position of the HOMO and LUMO levels **2–4** were estimated from their oxidation and reduction potentials (Table 3) and are in good agreement with those predicted by TD-DFT calculations (see Table S5). The coordination of gold(I) induced a decrease of the band gap, being 2.85 eV for **L** and 2.7 eV for gold(I) complexes **2–4**. This behaviour is well reproduced by calculations. The energy of HOMO and LUMO levels are in appropriate range for application as emissive layers in OLEDs [52].

2.6. Solvatochromism

The absorption and emission spectra of the compounds have been recorded in seven different solvents that cover a wide range of polarities (Fig. 7, S23-S25 and S30-32). The solvents used in this work together with their respective empirical solvent polarity parameters (α, β, π*, n) employed in some of the correlations are summarized in Table 4.

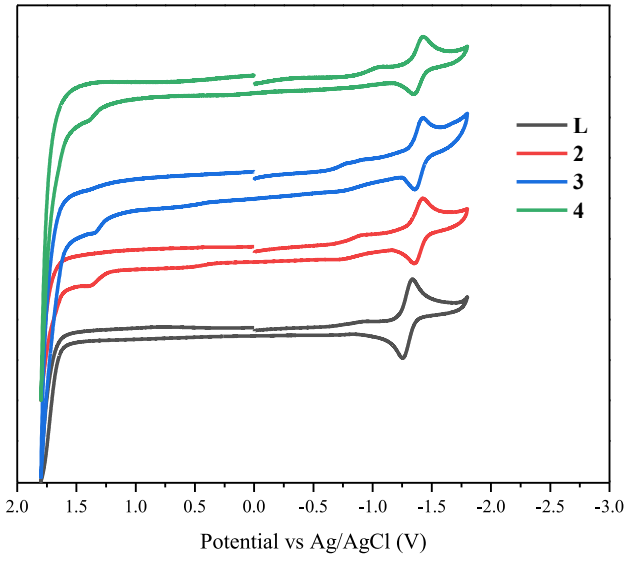

Fig. 6. Cyclic voltammogram of **L** and **2–4** in CH_2Cl_2 solution ($c = 1 \times 10^{-3}$ M) containing 0.1 M tetra-n-butylammonium hexafluorophosphate ($TBAPF_6$) of supporting electrolyte at a scan rate 100 mV/s.

As can be seen in Fig. 7, S23-S25 and S30-32, while absorption spectra are not significantly affected by the solvent polarity, a clear dependence on the solvent is observed in the emission spectra, presenting a large shift in the emission maxima between hexane and methanol (*ca.* 60 nm). No significant changes are also recorded in the corresponding excitation spectra (Figs. S26–S29). This behaviour is in agreement with other BTD-containing donor-acceptor chromophores [46]. Additionally, the polarity of the solvents induces a quenching on the emission intensity due to the stabilization of the polarized excited state by solvation from polar solvent molecules and induces an increase of the non-radiative deactivation pathway [38,40].

In order to estimate the excited state polarity, the recorded changes in the fluorescence emission with solvents of different polarizabilities

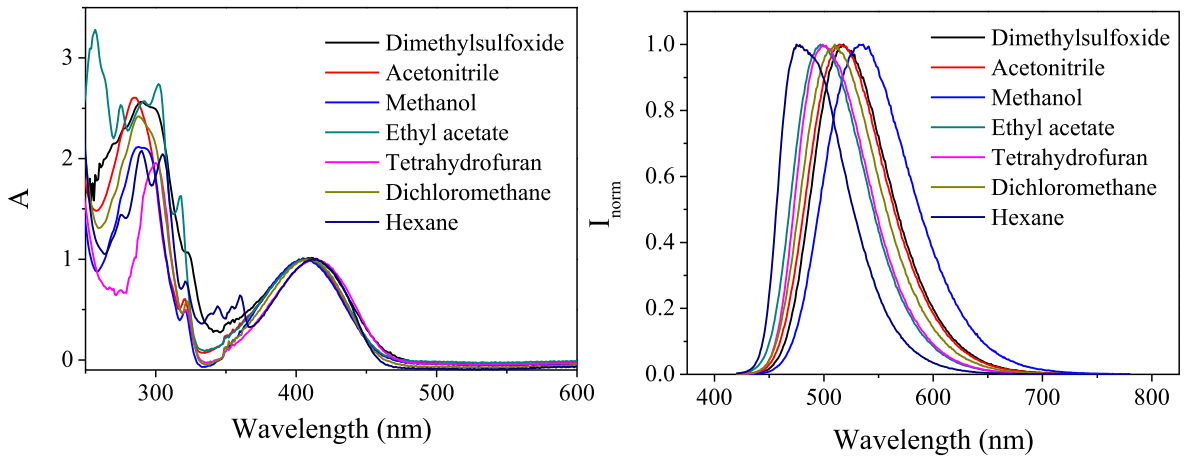

Fig. 7. Normalized absorption (left) and emission (right) spectra of compound **3** recorded in solvents with different polarity.

Table 3
Electrochemical data of **L** and **2–4**.

Compound	E_{ox} (V)	E_{red} (V)	E_{HOMO} (eV)	E_{LUMO} (eV)	E_{GAP} (eV)	λ_{onset} (nm)	$E_{GAP\ opt}$ (eV)
L	–	−1.292	−5.920	−3.070	–	435	2.85
2	1.38	−1.384	−5.739	−2.975	2.764	459	2.7
3	1.33	−1.389	−5.689	−2.970	2.719	458	2.7
4	1.38	−1.386	−5.739	−2.973	2.766	459	2.7

Table 4
α, β, π*, n Parameters for the solvents used [50].

Solvent	α	β	π*	μ	ε_r	n
Acetonitrile	0.19	0.40	0.66	13.0	35.94	1.3442
Ethyl acetate	0	0.45	0.55	5.9	6.02	1.3722
Dichloromethane	0.3	0	0.82	3.8	8.93	1.4241
Dimethylsulfoxide	0	0.76	1	13.5	46.45	1.4793
n-Hexane	0	0	−0.11	0	1.88	1.3749
Methanol	0.98	0.66	0.60	9.6	32.66	1.3288
Tetrahydrofuran	0	0.55	0.55	5.8	7.58	1.4072

where analyzed by means of the Lippert-Mataga equation (equation 1). This equation expresses the magnitude of the Stokes shift in terms of changes in the molecular dipole moment and the radius of the Onsager cavity.

$$\tilde{\upsilon}_a - \tilde{\upsilon}_f = \Delta f \frac{1}{4\pi\varepsilon_0} \frac{2(\mu_E - \mu_G)^2}{hca^3} + constant \qquad \text{(equation1)}$$

where $\tilde{\upsilon}_a$ and $\tilde{\upsilon}_f$ are the respective absorption and emission energies in wavenumbers, ε_0 is the permittivity, μ_E and μ_G are, respectively, the magnitudes of excited and ground state dipole moments, h is the Planck's constant, c is the speed of the light and a is the Onsager cavity radius (calculated from the van der Waals volume) [51]. The orientational polarizability Δf is defined as

$$\Delta f = \left[\frac{\varepsilon - 1}{2\varepsilon + 1} - \frac{n^2 - 1}{2n^2 + 1}\right] \qquad \text{(equation2)}$$

where ε and n are solvent dielectric constant and refractive index respectively.

The plots of the Stokes' shift versus the orientational polarizability Δf are shown in Fig. 8 and the corresponding slopes and the value of the variation of the dipolar moment and the Onsager cavity radius are represented in Table 5.

A positive correlation between the Stoke Shift and the orientational

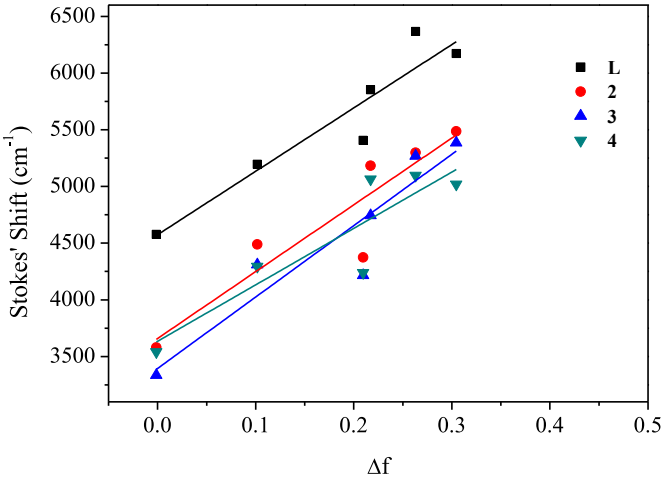

Fig. 8. Lippert-Mataga plots determined for **L** and gold(I) complexes **2–4**.

polarizability factor implies an ICT mechanism in the excited state. As can be observed in Table 5, gold(I) complexes **2–4** show larger change in the dipole moment than the ligand **L**, being more important for larger (and more polarizable) molecules. This observation indicates that the molecules are significantly more polar in the excited state than in the ground state [52,53]. Hence, the interaction between the compound and the solvent becomes stronger in the excited state and lead also to a quenching of the luminescence at higher solvent polarities [53,54]. The better correlation between the Δf and the Stokes' shift obtained for **L**, **2** and **3** ($R^2 \geq 0.85$) means a minor influence of the specific solvent effects in the excited state stability and the ICT transition [54]. Dichloromethane is the solvent with worse fitting in all cases suggesting that the influence of this solvent is larger. Additionally, methanol has been removed from the fitting since it is the only solvent than can be involved in hydrogen bonding processes.

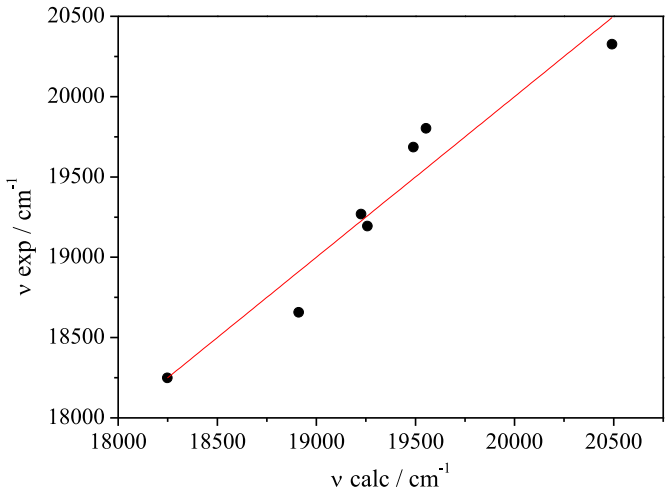

Fig. 9. Plot of υ^{-}_{exp} vs. υ^{-}_{calc} for emission data of compound **4**.

Table 5
Lippert-Mataga slope, variation of the dipolar moment and Onsager cavity radius data of **L** and **2–4.**

Compound	Slope (cm^{-1})	a (Å)	μ_E - μ_G (D)	R^2
L	5590	4.39	6.85	0.89
2	5892	4.89	8.26	0.85
3	6293	5.25	9.51	0.87
4	4976	5.58	9.26	0.80

The multiparametric Kamlet-Taft method was applied in order to analyse in more detail the interaction between the compounds and the solvent. With this analysis, absorption and emission energies are correlated with different solvent properties according to equation (3).

$$\overline{\nu} = \overline{\nu_0} + a\alpha + b\beta + p(\pi^* + d\delta) \quad \text{(equation3)}$$

where $\overline{\nu_0}$ corresponds to the value of the absorption or the emission energies for a reference solvent; α is the index related to the solvent ability to act as a hydrogen-bond donor (or electron pair acceptor) toward a solute; β corresponds to the ability of bulk solvents to behave as a hydrogen-bond acceptors (or electron-pair donors); π* is the index of the solvent polarity/polarizability which indicates the solvent ability to stabilize a neighbouring charge or dipole through non-specific dielectric interactions and finally, δ is the polarizability correction factor for different solvents. Considering that, often, the contribution of δ is negligible equation (3) can be simplified as

$$\overline{\nu} = \overline{\nu_0} + a\alpha + b\beta + p\pi^* \quad \text{(equation4)}$$

Linear plots of υ^{-}_{exp} versus υ^{-}_{calc}, (Fig. 9 and S33-S39), have been obtained for all compounds and the fitted parameters (υ^{-}_{0}, a, b and p), as well as slope and correlation coefficient are presented in Table 5.

Plots of υ^{-}_{exp} versus υ^{-}_{calc} yield slopes of 1 and good correlation coefficients are obtained in all cases. It can be observed that the solvatochromism in the emission of all the compounds is essentially reflected in the "a" and "p" solute parameters (see Table 6), that is ascribed to a larger sensitivity to the H-bond donor (or electron pair acceptor) of the solvent towards a solute and the polarity/polarizability of solvent respectively [55,56].

2.7. Water acetonitrile mixtures

The twisted conformation between the two aromatic rings of BTD found in the crystal structure together with the strong influence that the environment exerts on the light emitting properties of BTD derivatives, encouraged us to explore possible aggregation induced emission (AIE) phenomena in our systems. Please note that although there are some examples in the literature, BTDs have been scarcely explored regarding AIE phenomenon [17–19].

With this goal in mind, emission spectra and luminescence quantum yields, and lifetimes were measured in acetonitrile and in acetonitrile/water mixtures with increasing water contents. The obtained data are summarized in Tables 7 and 8. Compound **4** could not be studied likewise due to the lack of solubility of this compound in the presence of small amounts of water.

A decrease and slight broadening in absorption bands together with a slight increase on the baseline is detected for all compounds when the water contents increases, in agreement with the aggregation process (Figs. S40–S42) [16].

In acetonitrile solution, the gold complex **3** containing the bulkiest phosphane, shows a QY value above 90% (0.93) higher than that of the uncoordinated ligand **L** and to the best of our knowledge, represents the largest quantum yield recorded in the literature for gold(I) BTD complexes. The enhancement in the QY upon complexation has been previously observed in dichloromethane solution, although in acetonitrile the increase upon complexation is significantly higher (from 4% to 12%). A value above 90% can also be recorded for **L** in aggregated form (25–50% water contents) but not in pure solvent. In this case, the observed increase of the quantum yield may be attributed to the AIE mechanism that is dominating the effect of the solvent polarity [42]. AIE induces also an increase on the QY of **2** in aggregated form but in a lower extent (83% efficiency). It is expected that the resulting aggregates provide a hydrophobic cavity inside the aggregated structure that restricts solvation and eases radiative emission, resulting as an increase on the emission intensity. This increase and red-shift of the emission in **L** and **2** is observed up to 50% of water contents while a quenching effect is then observed. This behaviour may be attributed to the increased polarity of the solvent mixture and stabilization of the charge-transfer state, according to the literature [57], but also to the observed aggregation.

On the other hand, while AIE is detected for both **L** and complex **2**, the contrary effect, aggregation caused quenching (ACQ), was recorded for **3**, the compound showing the largest contribution on the dipolar moment in the excited state as reflected by the μ_E - μ_G value (see above, Table 4) and the lowest angle torsion predicted by TD-DFT calculations (see Table S6). In this case a ACQ is accompanied by a blue-shift at 75% of water contents, as previously observed in other BTD derivatives [42].

Interestingly we have been able to achieve near unity quantum yields in two of our compounds by modulation of the solvent (50% acetonitrile: water contents for **L** and pure acetonitrile solutions for **3**). These values are, in the case of **3** and, to the best of our knowledge, much higher than others previously reported in the literature for gold(I)-ethynylBTD

Table 6
υ^{-}_{0}, a, b and p values, in cm^{-1}, as well as slope and correlation coefficients obtained from Kamlet-Taft multiparametric of the emission data of **L** and **2–4.**

Compound	υ^{-}_{0}	a	b	p	Slope	r^2
L	21754	−1083	−684	−1382	1.0	0.94
2	20471	−1351	−605	−1038	1.0	0.98
3	20676	−1121	−690	−937	1.0	0.95
4	20383	−1145	−631	−992	1.0	0.93

Table 7
Quantum yields (%) of **L**, **2–4** in acetonitrile and in acetonitrile/water mixtures with increasing water fractions.

Compound	Acetonitrile	25% H_2O	50% H_2O	75% H_2O
L	81	96	97	19
2	76	83	77	14
3	93	84	74	18
4	87	–	–	–

Table 8
Lifetimes (ns) of **L**, **2** and **3** in acetonitrile and in acetonitrile/water mixtures with increasing water fractions.

Compound	Acetonitrile	25% H_2O	50% H_2O	75% H_2O
L	9.8	13.7	14.1	13
2	10.8	11.4	12.6	12.6
3	11.1	11.1	11.6	12.1

complexes (that are in the range of 60–70%) [11], and, in the case of **L**, comparable with other few organic BTD compounds [10].

Emission lifetimes are also affected by the presence of water being larger with increasing water contents in the solution. This effect is more noticeable for the pure organic counterpart **L**. The global effect of the aggregation on the photophysical properties may be seen in the variations of the k_r and k_{nr} rate constants (Table 9 and Fig. S46) where it seems that the environment is affecting significantly these parameters only above 50% with a significant decrease (k_r) or increase (k_{nr}) of these values. Thus, it is important to take this information into consideration, since longer lifetimes may be achieved by favoring aggregation but this is accompanied by a favored deactivation pathway, as reflected in the higher k_{nr} values. Nevertheless, the quantum yields at the highest water contents are still moderate (15–20%). Thus, aggregation gives an easy way to modulate the photophysical properties of BTD derivatives with the adequate and desired balance between lifetimes and quantum yields.

The formation of aggregates was verified by Dynamic Light Scattering (DLS) experiments. Two groups of aggregates can be detected for **L** when the water contents increases (25% and 50%) and up to 75% water where the aggregates equilibrate in only one group (*ca.* 200 nm, Fig. S42). On the other hand, more homogeneous samples have been detected in gold(I) complexes with just one group of aggregates. That is, the presence of gold(I) may govern the aggregation processes with preferred intermolecular contacts with respect to **L** (Figs. S47–S49) probably due to the establishment of aurophilic contacts in solution although they are not identified in the solid state (X-ray crystal structures). The sizes detected for the gold complexes change with water composition but reached a final value of *ca.* 200 nm at 75% of water contents, which is similar to the previously detected for **L** and to other BTD aggregates described in the literature [38].

2.8. Hybrid materials

The new compounds were dispersed in different polymeric matrices of different nature in an attempt to favour the radiative pathways (cellulose, polymethylmethacrylate (PMMA), polystyrene (PS) and the cyclic olefin copolymer, Zeonex). Small amounts (<3%) of the organic chromophores are usually enough to confer these hybrid materials the desired light emitting properties while maintaining the interesting mechanical properties of the polymeric matrix. The emission spectra of the compounds dispersed in these matrixes show a blue shift of the emission maxima (around 10 nm) in all the samples when they are compared with the emission recorded in the solid state (Table 10 and Figs. S50–S53) with the sample more shifted to the red for the most polar cellulose environment.

Quantum yields and lifetimes for the different samples are summarized in Tables 11 and 12. In general trends, there is a clear increase of the quantum yields and emission lifetimes when the compounds are introduced in the thin films with respect to the more compact solid state. The quantum yields are also larger than those previously recorded in solution and in the same order or slightly larger than those recorded in acetonitrile:water mixtures reaching almost 100% in PMMA, PS and Zeonex matrixes for **L**, **2** and **3**. The largest values (97%) has been recorded for the gold(I) complex **3** in PS, being the highest QY for gold(I) BTD complexes described in the literature. For the best of our knowledge, there are no precedents in the literature of gold(I) BTD derivatives in polymer matrixes and, interestingly, their inclusion in this environments favors near-unity quantum yields. This environment favors much more the radiative deactivation pathway of gold(I) complexes with respect to the organic part **L**. Lifetimes values are in all cases longer than those previously recorded in the solid, as previously observed in other gold(I) emitters [23,58,59]. Additionally, it can be observed that the values of the gold(I) complexes are much more similar to those recorded for **L** with respect to the previous values recorded in solid, except in the case of **4**, containing the more steric hindrance phosphane.

An important point to be highlighted is that the introduction of the compounds in thin films decreases the k_{nr} rate constants mainly for gold (I) complexes (Table 13), although some effect has been also detected for **L** in Zeonex. Thus, the introduction of the compounds in matrices enhances the luminescent properties in an intermediate aggregation state between solid state and solution. Additionally, although similar quantum yields have been observed in water/acetonitrile mixtures, the formation of these hybrid materials favors the radiative relaxation (larger k_r values) and blocks the non-radiative pathways (lower k_{nr} values) in one order of magnitude, mainly for gold(I) complexes.

Table 9
Radiative and non-radiative constants (μs^{-1}) of **L**, **2** and **3** in acetonitrile and in acetonitrile/water mixtures with increasing water fractions.

Compound	Acetonitrile		25% H_2O		50% H_2O		75% H_2O	
	k_r	k_{nr}	k_r	k_{nr}	k_r	k_{nr}	k_r	k_{nr}
L	83	19	70	3	68	2	15	62
2	70	22	73	15	61	18	43	36
3	84	6	76	14	64	22	15	68

Table 10
Emission maxima of **L** and **2–4** in solid state and in matrixes of cellulose, poly methyl methacrylate (PMMA), polystyrene (PS) and Zeonex.

Compound	Solid	Cellulose	PMMA	PS	Zeonex
L	485	477	467	470	467
2	517	503	497	498	501
3	514	504	494	497	498
4	517	499	501	498	500

Table 11
Quantum yield (%) of **L** and **2–4** in solid state and in matrixes of cellulose, poly methyl methacrylate (PMMA), polystyrene (PS) and Zeonex.

Compound	Φ_{fl} (solid)	Φ_{fl} (Cellulose)	Φ_{fl} (PMMA)	Φ_{fl} (PS)	Φ_{fl} (Zeonex)
L	36	91	96	95	93
2	5.6	91	95	94	92
3	24	89	94	97	96
4	18	31	41	41	45

Table 12
Lifetime (ns) of **L** and **2–4** in solid state and in matrixes of cellulose, polymethylmethacrylate (PMMA), polystyrene (PS) and Zeonex.

Compound	τ_{fl} (solid)	τ_{fl} (Cellulose)	τ_{fl} (PMMA)	τ_{fl} (PS)	τ_{fl} (Zeonex)
L	5.8	9.69	9.07	8.01	8.4
2	3.92	8.32	8.54	7.75	8.51
3	2.01	7.82	8.83	7.09	7.69
4	3.78	6.79	3.89	3.62	4.32

3. Conclusions

The coordination of the new ethynyl-BTD ligand (**L**) to a gold(I) atom gives rise to a new family of compounds with interesting luminescent properties. The resulting photophysical properties can be modulated not only by the BTD core but also by the solvent polarity and the possibility

Table 13
Radiative and non-radiative constants (μs^{-1}) of **L** and **2–4** in solid state and in matrixes of cellulose, poly methyl methacrylate (PMMA), polystyrene (PS) and Zeonex.

Compound	Solid		Cellulose		PMMA		PS		Zeonex	
	k_r	k_{nr}	k_r	k_{nr}	k_r	k_{nr}	k_r	k_{nr}	k_r	k_{nr}
L	62	110	94	9	106	4	119	6	111	8
2	14	241	251	25	111	6	121	8	108	9
3	119	378	114	14	106	7	137	4	125	5
4	48	217	46	102	105	152	113	163	104	127

of aggregation, which may be favored through different type of weak interactions. The resulting compounds display very high fluorescence quantum yields that may depend on the solvent, being 80% in dichloromethane and, in some cases, near unity in acetonitrile. The near unity quantum yields may be also modulated through changes on the environment. In this way, detailed studies have been carried out in acetonitrile:water mixtures (to favour aggregation processes at increasing water contents), in solid state and through dispersion of the compounds in organic matrixes. The highest QY values have been recorded for the gold(I) complex **3** in PS (97%) being the highest value recorded for a gold(I)-BTD compound. Changes on the environment also affect the fluorescence lifetimes, being larger in more aggregated samples (highest water contents in acetonitrile:water mixtures). Thus, aggregation has been observed as an effective and easy way to modulate the resulting photophysical properties mainly regarding QY and lifetimes.

The inclusion of the compounds within organic matrixes clearly favors the radiative deactivation pathways of the compounds as observed with a denoted increase of k_r and decrease of k_{nr} values.

The high QY values shown by these complexes together with the environmental sensitivity of their light-emitting properties represent a promising property toward their application in fields such as sensing, bioimaging or light emitting diodes.

4. Experimental section

4.1. General procedures

All manipulations have been performed under prepurified N_2 using standard Schlenk techniques. All solvents have been distilled from appropriated drying agents. Commercial reagents triethylphosphine (PEt_3, Aldrich 99%), triphenylphosphine (PPh_3, Aldrich 99%), tri-1-naphthylphosphine ($PNaph_3$ Aldrich, 97%) were used as received.

4.2. Physical measurements

Infrared spectra have been recorded on a FT-IR 520 Nicolet Spectrophotometer. ^{1}H NMR (δ(TMS) = 0.0 ppm), ^{31}P{^{1}H}-NMR (δ(85% H_3PO_4) = 0.0 ppm) spectra have been obtained on a Varian Mercury 400 and Bruker 400 (Universitat de Barcelona). ElectroSpray-Mass spectra (+) has been recorded on a Fisons VG Quatro spectrometer (Universitat de Barcelona). Absorption spectra have been recorded on a Varian Cary 100 Bio UV- spectrophotometer and emission spectra on a Horiba-Jobin-Yvon SPEX Nanolog spectrofluorimeter (Universitat de Barcelona). Luminescent quantum yields were recorded using an Absolute PL quantum yield spectrometer from Hamamatsu Photonics upon excitation the samples at 400 nm. Fluorescence lifetimes were measured via the time-correlated single-photon counting technique (TCSPC) using DeltaPro fluorescence lifetime System from Horiba upon excitation of the sample with a 390 nm nanoLED. Cyclic voltammetry (CV) experiments were performed on a Bioanalytical Systems Inc. (BASI) Epsilon electrochemical workstation in a three-electrode cell at room temperature under nitrogen atmosphere. Crystal of **3** and **4** showing well defined faces were mounted Bruker Kappa Apex II (X8 APEX) diffractometer equipped with a Mo INCOATED microsource. Diffraction data were collected exploring over a hemisphere of the reciprocal space in a combination of φ and ω scans to reach a resolution of 0.86 Å, using a Bruker APEXII software suite (APEX2; Bruker-AXS: Madison, WI, 2006). The structures were solved by the Multan and Fourier methods. Most of the calculations were carried out with APEXII software for data collection and reduction, and OLEX2 for structure solution and refinements. CCDC 2091781–2091782 contain the supplementary crystallographic data for this paper. These data can be obtained free of charge via www.ccdc.cam.ac.uk/data_request/cif, or by emailing data_request@ccdc.cam.ac.uk, or by contacting The Cambridge Crystallographic Data Centre, 12 Union Road, Cambridge CB2 1EZ, UK; fax: +44 1223 336033.

4.3. Theoretical calculations

Density functional calculations were carried out using the Gaussian 09 package [61]. The hybrid density functional known as B3LYP was applied [62,63]. Effective core potential (ECPs) were used to represent the innermost electrons of the gold atom and the basis set of valence triple-ζ quality with extra d-polarization function [64]. A similar description was used for all main group elements [65]. Excited states were obtained from the time-dependent density functional theory (TDDFT) implemented in Gaussian 09 [66].

4.4. Synthesis and characterization

4.4.1. Synthesis of 4-ethynyl-7-(4-nonylphenyl)benzo[c] [1,2,5] thiadiazole (L)

A mixture of 4-bromo-7-(4-nonylphenyl)benzo[*c*] [1,2,5]thiadiazole (200 mg, 0.48 mmol), CuI (4.6 mg, 0.024 mmol) and $Pd(dppf)_2Cl_2$ (17.6 mg, 0.024 mmol) in 6 ml of a 1:1 mixture triethylamine:THF was degassed, and then, ethynyl trimethylsilane (0.73 ml, 0.52 mmol) was added. The solution was irradiated with an Anton Paar microwave irradiator (CEM) at 120 °C (80W) for 120 min. After cooling to room temperature, the mixture was diluted with CH_2Cl_2, washed with water, and dried ($MgSO_4$); the solvent was then evaporated and the residue was purified by chromatography with CH_2Cl_2/hexane (1:3) to give a yellow solid 4-(4-nonylphenyl)-7-((trimethylsilyl)ethynyl)benzo[*c*] [1,2,5] thiadiazole (177 mg, 85%).

^{1}H NMR ($CDCl_3$) δ 7.86 (d, J = 8.2 Hz, 2H), 7.83 (d, J = 7.4 Hz, 1H), 7.64 (d, J = 7.4 Hz, 1H), 7.34 (d, J = 8.2 Hz, 2H), 2.69 (t, J = 7.7 Hz, 2H), 1.86–1.56 (m, 2H), 1.51–1.16 (m, 12H), 1.00–0.80 (m, 3H), 0.35 (s, 9H).^{13}C NMR ($CDCl_3$) δ 155.7, 153.3, 144.4, 136.2, 135.4, 134.1, 129.3, 129.0, 127.3, 114.02, 80.2, 80.0, 36.0, 32.0, 31.6, 29.7, 29.5, 22.8, 14.3. FAB MS *m/z* 434.71 (M^+); HRMS (FAB) calcd for $C_{26}H_{34}N_2SSi$: 434.2212, found: 434.2205.

A mixture of 4-(4-nonylphenyl)-7-((trimethylsilyl)ethynyl)benzo[*c*] [1,2,5]thiadiazole (100 mg, 0.23 mmol) and KF (138 mg, 3.45 mmol) was stirred for 12h at room temperature in 8 ml of a 1:1 mixture of THF: MeOH. Then the mixture was diluted with CH_2Cl_2, washed with water, and dried ($MgSO_4$); the solvent was then evaporated to give **L** as a yellow solid (75 mg, 90%) .^{1}H NMR ($CDCl_3$) δ 7.89 (d, J = 7.2 Hz, 2H), 7.84 (d, J = 7.8 Hz, 1H), 7.67 (d, J = 7.3 Hz, 1H), 7.35 (d, J = 7.9 Hz, 2H), 3.61 (s, 1H), 2.69 (t, J = 7.7 Hz, 2H), 2.03 (t, J = 7.1 Hz, 2H), 1.41–1.17 (m, 12H), 0.88 (t, J = 6.5 Hz, 3H). ^{13}C NMR ($CDCl_3$) δ 155.6, 153.2, 144.2, 135.7, 134.2, 129.3, 129.0, 127.2, 114.2, 83.6, 79.7, 36.0, 32.1, 31.6, 29.6, 29.5, 29.3, 29.1, 22.8, 14.3. FAB MS *m/z* 362.53 (M^+); HRMS (FAB) calcd for $C_{23}H_{26}N_2S$: 362.1817, found: 362.1825.

4.4.2. Synthesis of [Au(4-ethynyl-7-(4-nonylphenyl)benzo[c] [1,2,5] thiadiazole)]$_n$ (1)

Sodium acetate (0.0102 g, 0.12 mmol) and [AuCl(tht)] (0.0191 g, 0.06 mmol) were added to a stirring solution of **L** (0.0212 g, 0.06 mmol) in CH_2Cl_2/MeOH (1:1) (10 mL) under N_2 atmosphere at room temperature. After stirring for 30 min the resulting orange suspension was filtered, washed with CH_2Cl_2/MeOH (1:1) (3 × 5 mL), and dried under vacuum. Yield 63% (0.023 g). IR (KBr, cm^{-1}): ν(C≡C): 1970.

4.4.3. Synthesis of [Au(4-ethynyl-7-(4-nonylphenyl)benzo[c] [1,2,5] thiadiazole)(PEt$_3$)] (2)

31 μL of a solution 1.0 M of PEt_3 in THF was added to a stirring suspension of **1** (0.017 g, 0.030 mmol) in dichloromethane (10 mL) under N_2 atmosphere at room temperature. After stirring 1h the resulting yellow solution was concentrated to half volume and hexane (10 mL) was then added in order to favour precipitation. The resulting yellow solid was filtered and dried under vacuum. Yield 75% (0.015 g). $^{31}P\{^1H\}$-NMR ($CDCl_3$, ppm): 37.6. ^1H NMR ($CDCl_3$, ppm): 0.88 (t, J = 6.8 Hz, 3H), 1.15–1.4 (m, 21H), 1.66 (m, 2H), 1.83 (m, 6H), 2.67 (t, J = 7.7 Hz, 2H), 7.32 (d, J = 8Hz, 2H), 7.60 (d, J = 7.4 Hz, 1H), 7.78 (d, J = 7.3 Hz, 1H), 7.84 (d, J = 8Hz, 2H).). ^{13}C NMR ($CDCl_3$): 127.9, 127.6, 126.6, 34.8, 30.9, 30.4, 28.5, 28.4, 28.3, 21.7, 17.0, 16.7, 13.1, 7.8. IR (KBr, cm^{-1}): ν(C≡C): 2108. ESI-MS (+) m/z: 677.2391 ($[M + H]^+$, calc: 677.2315).

4.4.4. Synthesis of [Au(4-ethynyl-7-(4-nonylphenyl)benzo[c] [1,2,5] thiadiazole)(PPh$_3$)] (3)

Solid PPh_3 (0.0086 g, 0.033 mmol) was added to a stirring suspension of **1** (0.0185 g, 0.033 mmol) in dichloromethane (10 mL) under N_2 atmosphere at room temperature. After stirring 1h the resulting yellow solution was concentrated to half volume and hexane (10 mL) was then added in order to favour precipitation. The resulting yellow solid was filtered and dried under vacuum. Yield 74% (0.025 g). $^{31}P\{^1H\}$-NMR ($CDCl_3$, ppm): 42.1. ^1H NMR ($CDCl_3$, ppm): 0.88 (t, J = 6.8 Hz, 3H), 1.15–1.4 (m, 12H), 1.66 (m, 2H), 2.67 (t, J = 7.7 Hz, 2H), 7.33 (d, J = 8Hz, 2H), 7.43–7.63 (m, 16H), 7.81 (d, J = 7.4 Hz, 1H), 7.85 (d, J = 8Hz, 2H).). ^{13}C NMR ($CDCl_3$): 134.4, 134.3, 132.7, 131.6, 129.2, 129.1, 129.0, 128.7, 127.7, 35.8, 31.9, 31.4, 29.6, 29.4, 29.3, 22.7, 14.1. IR (KBr, cm^{-1}): ν(C≡C): 2110. ESI-MS (+) m/z: 821.2392 ($[M + H]^+$, calc: 821.2315).

4.4.5. Synthesis of [Au(4-ethynyl-7-(4-nonylphenyl)benzo[c] [1,2,5] thiadiazole)(Tri-1-naphthylphosphine)] (4)

Solid tri-1-naphthylphosphine (0.023 g, 0.056 mmol) was added to a stirring suspension of **1** (0.0303 g, 0.054 mmol) in dichloromethane (10 mL) under N_2 atmosphere at room temperature. After stirring 1h the resulting yellow solution was concentrated to half volume and hexane (10 mL) was then added in order to favour precipitation. The resulting yellow solid was filtered and dried under vacuum. Yield 76% (0.042 g). $^{31}P\{^1H\}$-NMR ($CDCl_3$, ppm): 21.8. ^1H NMR ($CDCl_3$, ppm): 0.87 (t, J = 6.8 Hz, 3H), 1.15–1.4 (m, 12H), 1.66 (m, 2H), 2.67 (t, J = 7.7 Hz, 2H), 7.28–7.37 (m, 8H), 7.50–7.62 (m, 4H), 7.71 (d, J = 7.4 Hz, 1H), 7.82 (d, J = 8 Hz, 2H), 7.97 (d, J = 7.9 Hz, 3H), 8.05 (d, J = 7.6 Hz, 3H), 8.83 (d, J = 8.3 Hz, 3H). ^{13}C NMR ($CDCl_3$): 156.2, 153.1, 143.2, 139.1, 137.7, 135.1, 135.0, 134.7, 134.3, 134.2, 134.1, 134.0, 133.1, 132.7, 129.1, 128.9, 127.7, 127.6, 127.1, 126.9, 126.8, 125.2, 125.1, 124.2, 123.7, 117.6, 99.4, 99.1, 35.8, 31.9, 31.4, 29.6, 29.5, 29.4, 29.3, 22.7, 14.1. IR (KBr, cm^{-1}): ν(C≡C): 2108. MALDI-TOF (+) m/z: 1021.2 ($[M + H + CH_3OH + H_2O]^+$, calc: 1021.3).

4.4.6. Preparation of matrixes doped with L and 2–4 complexes

Cellulose, PMMA, PS and Zeonex (Zeon Corporation, Japan) were used as matrix polymers. The films were prepared via drop-casting, using a mixture of dopant and host (Cellulose, PMMA, PS or Zeonex). Polymer solutions were prepared as follows: PMMA (MW 120000, 300 mg/mL solution in dichloromethane), PS (MW 45000, 350 mg/mL solution in dichloromethane). Cellulose (MW 30000, 200 mg/mL in acetone), Zeonex (200 mg/mL in chloroform). To a 100 μL of polymer solution was added to the same volume a solution of the sample at a concentration of 20 μg/mL. The films were drop-cast onto a quartz substrate at room temperature to avoid any thermal annealing.

Author contribution statement

Andrea Pinto: synthesis of the gold(I) complexes, luminescent studies, solvatochromism, DFT calculations, synthesis of luminescent matrixes, help on writing of the manuscript. Marcelo Echeverri: synthesis of L, electrochemical studies. Berta Gómez-Lor: supervision of synthesis of L and electrochemical studies, collaboration on the writing of the manuscript. Laura Rodríguez: global supervision, in particular of gold(I) complexes, matrixes and luminescence studies. Writing of the manuscript.

Declaration of competing interest

The authors declare that they have no known competing financial interests or personal relationships that could have appeared to influence the work reported in this paper.

Acknowledgements

The authors are grateful to Projects PID2019-104121GB-I00 and PID2019-104125RB-I00 funded by the Ministerio de Ciencia e Innovación of Spain MCIN/AEI/10.13039/501100011033. We are indebted to Zeon Europe GmbH for providing us with Zeonex 480. We gratefully acknowledge Dr Josefina Perles for solving the crystal structure of **3** and **4** and Prof. Gabriel Aullón and Ms. Araceli de Aquino for the help on the theoretical studies.

Appendix A. Supplementary data

Supplementary data to this article can be found online at https://doi.org/10.1016/j.dyepig.2022.110308.

References

[1] Bala I, Yadav RAK, Devi M, De J, Singh N, Kailasam K, Jayakumar J, Jou JH, Cheng CH, Pal SK. High-performing D–π–A–π–D benzothiadiazole-based hybrid local and charge-transfer emitters in solution-processed OLEDs. J Mater Chem C 2020;8:17009–15.

[2] Zhang D, Yang T, Xu H, Miao Y, Chen R, Shinar R, Shinar J, Wang H, Xu B, Yu J. Triphenylamine/benzothiadiazole-based compounds for non-doped orange and red fluorescent OLEDs with high efficiencies and low efficiency roll-off. J Mater Chem C 2021;9:4921–6.

[3] Chan KT, Tong GSM, To WP, Yang C, Du L, Phillips DL, Che CM. The interplay between fluorescence and phosphorescence with luminescent gold(I) and gold(III) complexes bearing heterocyclic arylacetylide ligands. Chem Sci 2017;8:2352–64.

[4] Bartolini M, Gombac V, Sinicropi A, Reginato G, Dessì A, Mordini A, Filippi J, Montini T, Calamante M, Fornasiero P, Zani L. Tuning the properties of benzothiadiazole dyes for efficient visible light-driven photocatalytic H 2 production under different conditions. ACS Appl Energy Mater 2020;3:8912–28.

[5] Zhang J, Konsmo A, Sandberg A, Wu X, Nyström S, Obermüller U, Wegenast-Braun BM, Konradsson P, Lindgren M, Hammarström P. Phenolic Bis-styrylbenzo[c]-1,2,5-thiadiazoles as probes for fluorescence microscopy mapping of Aβ plaque heterogeneity. J Med Chem 2019;62:2038–48.

[6] Godfroy M, Liotier J, Mwalukuku VM, Joly D, Huaulmé Q, Cabau L, Aumaitre C, Kervella Y, Narbey S, Oswald F, Palomares E, González Flores CA, Oskam G, Demadrille R. Benzothiadiazole-based photosensitizers for efficient and stable dye-sensitized solar cells and 8.7% efficiency semi-transparent mini-modules. Sustain Energy Fuels 2021;5:144–53.

[7] Li Y, Scudiero L, Ren T, Dong WJ. Synthesis and characterizations of benzothiadiazole-based fluorophores as potential wavelength-shifting materials. J Photochem Photobiol A Chem 2012;231:51–9.

[8] Neto BAD, Lapis AAM, da Silva Júnior EN, Dupont J. 2,1,3-Benzothiadiazole and derivatives: synthesis, properties, reactions, and applications in light technology of small molecules. Eur J Org Chem 2013;2013:228–55.

[9] Echeverri M, Ruiz C, Gámez-Valenzuela S, Alonso-Navarro M, Gutierrez-Puebla E, Serrano JL, Ruiz Delgado MC, Gómez-Lor B. Stimuli-responsive benzothiadiazole derivative as a dopant for rewritable polymer blends. ACS Appl Mater Interfaces 2020;12:10929–37.

[10] Rietsch P, Sobottka S, Hoffmann K, Hildebrandt P, Sarkar B, Resch-Genger U, Eigler S. Identification of the irreversible redox behavior of highly fluorescent benzothiadiazoles. ChemPhotoChem 2020;4:668–73.

[11] Goswami S, Winkel RW, Schanze KS. Photophysics and nonlinear absorption of gold(I) and platinum(II) donor–acceptor–donor chromophores. Inorg Chem 2015; 54:10007–14.

[12] Islam SN, Sil A, Patra SK. Achieving yellow emission by varying the donor/ acceptor units in rod-shaped fluorenyl-alkynyl based π-conjugated oligomers and their binuclear gold(I) alkynyl complexes. Dalton Trans 2017;46:5918–29.

[13] Lima JC, Rodríguez L. Applications of gold(i) alkynyl systems: a growing field to explore. Chem Soc Rev 2011;40:5442–56.

[14] Pujadas M, Rodríguez L. Luminescent phosphine gold(I) alkynyl complexes. Highlights from 2010 to 2018. Coord Chem Rev 2020;408:213179.

[15] Lima JC, Rodríguez L. Supramolecular gold metallogelators: the key role of metallophilic interactions. Inorganics 2015;3:1–18.

[16] Pinto A, Svahn N, Lima JC, Rodríguez L. Aggregation induced emission of gold(I) complexes in water or water mixtures. Dalton Trans 2017;46:11125–39.

[17] Pazini A, Maqueira L, da Silveira Santos F, Jardim Barreto AR, dos S, Carvalho R, Valente FM, Back D, Aucélio RQ, Cremona M, Rodembusch FS, Limberger J. Designing highly luminescent aryloxy-benzothiadiazole derivatives with aggregation-induced enhanced emission. Dyes Pigments 2020;178:108377.

[18] Zhao Z, Deng C, Chen S, Lam JWY, Qin W, Lu P, Wang Z, Kwok HS, Ma Y, Qiu H, Tang BZ. Full emission color tuning in luminogens constructed from tetraphenylethene, benzo-2,1,3-thiadiazole and thiophene building blocks. Chem Commun 2011;47:8847–9.

[19] Zhao Z, Geng J, Chang Z, Chen S, Deng C, Jiang T, Qin W, Lam JWY, Kwok HS, Qiu H, Liu B, Tang BZ. A tetraphenylethene-based red luminophor for an efficient non-doped electroluminescence device and cellular imaging. J Mater Chem 2012; 22:11018–21.

[20] Bhagwat AA, Mohbiya DR, Avhad KC, Sekar N. Viscosity-active D-π-A chromophores derived from benzo[b]thiophen-3(2H)-one 1,1-dioxide (BTD): synthesis, photophysical, and NLO properties. Spectrochim Acta - Part A Mol Biomol Spectrosc 2018;203:244–57.

[21] Koshevoy IO, Lin CL, Karttunen AJ, Jänis J, Haukka M, Tunik SP, Chou PT, Pakkanen TA. Highly luminescent octanuclear AuI-CuI clusters adopting two structural motifs: the effect of aliphatic alkynyl ligands. Chem - A Eur J 2011;17: 11456–66.

[22] Echeverri M, Ruiz C, Gámez-Valenzuela S, Martín I, Ruiz Delgado MC, Gutiérrez-Puebla E, Monge MÁ, Aguirre-Díaz LM, Gómez-Lor B. Untangling the mechanochromic properties of benzothiadiazole-based luminescent polymorphs through supramolecular organic framework topology. J Am Chem Soc 2020;142: 17147–55.

[23] de Aquino A, Caparrós FJ, Aullón G, Ward JS, Rissanen K, Jung Y, Choi H, Lima JC, Rodríguez L. Effect of gold(I) on the room-temperature phosphorescence of ethynylphenanthrene. Chem - A Eur J 2021;27:1810–20.

[24] Svahn N, Moro AJ, Roma-Rodrigues C, Puttreddy R, Rissanen K, Baptista PV, Fernandes AR, Lima JC, Rodríguez L. The important role of the nuclearity, rigidity, and solubility of phosphane ligands in the biological activity of gold(I) complexes. Chem - A Eur J 2018;24:14654–67.

[25] Aguiló E, Moro AJ, Gavara R, Alfonso I, Pérez Y, Zaccaria F, Guerra CF, Malfois M, Baucells C, Ferrer M, Lima JC, Rodríguez L. Reversible self-assembly of water-soluble gold(I) complexes. Inorg Chem 2018;57:1017–28.

[26] Ferrer M, Mounir M, Rodríguez L, Rossell O, Coco S, Gómez-Sal P, Martín A. Effect of the organic fragment on the mesogenic properties of a series of organogold(I) isocyanide complexes. X-ray crystal structure of [Au(CCC$_5$H$_4$N)(CNC$_6$H$_4$O(O) CC$_6$H$_4$OC$_{10}$H$_{21}$)]. J Organomet Chem 2005;690:2200–8.

[27] Svahn N, Sanz I, Rissanen K, Rodríguez L. Supramolecular assemblies and photophysical properties of ionic homo- and heteronuclear metallophilic complexes. J Organomet Chem 2019;897:170–7.

[28] Gavara R, Pinto A, Donamaría R, Olmos ME, López de Luzuriaga JM, Rodríguez L. Polarized supramolecular aggregates based on luminescent perhalogenated gold derivatives. Inorg Chem 2017;56:11946–55.

[29] Ferrer M, Rodríguez L, Rossell O, Pina F, Lima JC, Bardia MF, Solans X. Linear ditopic acetylide gold or mercury complexes: synthesis and photophysic studiesX-ray crystal structure of PPh$_4$[Au(C≡CC$_5$H$_4$N)$_2$]. J Organomet Chem 2003;678: 82–9.

[30] Gavara R, Llorca J, Lima JC, Rodríguez L. A luminescent hydrogel based on a new Au(I) complex. Chem Commun 2013;49:72–4.

[31] Arcau J, Andermark V, Aguiló E, Gandioso A, Moro A, Cetina M, Lima JC, Rissanen K, Ott I, Rodríguez L. Luminescent alkynyl-gold(I) coumarin derivatives and their biological activity. Dalton Trans 2014;43:4426–36.

[32] Moro AJ, Rome B, Aguiló E, Arcau J, Puttreddy R, Rissanen K, Lima JC, Rodríguez L. A coumarin based gold(I)-alkynyl complex: a new class of supramolecular hydrogelators. Org Biomol Chem 2015;13:2026–33.

[33] Blanco MC, Cámara J, Fernández-Moreira V, Laguna A, Gimeno MC. Gold(I), phosphanes, and alkynyls: the perfect allies in the search for luminescent compounds. Eur J Inorg Chem 2018;2018:2762–7.

[34] García-Moreno E, Gascón S, Rodriguez-Yoldi MJ, Cerrada E, Laguna M. S - propargylthiopyridine phosphane derivatives as anticancer agents: characterization and antitumor activity. Organometallics 2013;32:3710–20.

[35] Jin M, Chung TS, Seki T, Ito H, Garcia-Garibay MA. Phosphorescence control mediated by molecular rotation and aurophilic interactions in amphidynamic crystals of 1,4-Bis[tri-(p -fluorophenyl)phosphane-gold(I)-ethynyl]benzene. J Am Chem Soc 2017;139:18115–21.

[36] Echeverri M, Martín I, Concellón A, Ruiz C, Anselmo MS, Gutiérrez-Puebla E, Serrano JL, Gómez-Lor B. Fluorescent and electroactive monoalkyl BTD-based liquid crystals with tunable self-assembling and electronic properties. ACS Omega 2018;3:11857–64.

[37] Pazini A, Maqueira L, Stieler R, Aucélio RQ, Limberger J. Synthesis, characterization and photophysical properties of luminescent non-symmetric 4-pyridyl benzothiadiazole derivatives. J Mol Struct 2017;1131:181–9.

[38] Ishi-i T, Hashimoto R, Ogawa M. Aggregation of naphthobisthiadiazole-based donor-acceptor-donor dyes that restrict quenching in solution and emit red light in polar aqueous media. Asian J Org Chem 2014;3:1074–82.

[39] Misra R, Gautam P, Jadhav T, Mobin SM. Donor–acceptor ferrocenyl-substituted benzothiadiazoles: synthesis, structure, and properties. J Org Chem 2013;78: 4940–8.

[40] Kato S, Matsumoto T, Shigeiwa M, Gorohmaru H, Maeda S, Ishi-i T, Mataka S. Novel 2,1,3-benzothiadiazole-based red-fluorescent dyes with enhanced two-photon absorption cross-sections. Chem - A Eur J 2006;12:2303–17.

[41] Chai Z, Wang J, Xie Y, Lin P, Li H, Chang K, Xu T, Mei A, Peng Q, Wang M, Han H, Li Q, Li Z. Modulation of acceptor position in organic sensitizers: the optimization of intramolecular and interfacial charge transfer processes. ACS Appl Mater Interfaces 2019;11:27648–57.

[42] Jadhav T, Dhokale B, Misra R. Effect of the cyano group on solid state photophysical behavior of tetraphenylethene substituted benzothiadiazoles. J Mater Chem C 2015;3:9063–8.

[43] Goswami S, Wicks G, Rebane A, Schanze KS. Photophysics and non-linear absorption of Au(I) and Pt(II) acetylide complexes of a thienyl-carbazole chromophore. Dalton Trans 2014;43:17721–8.

[44] Abeywickrama CS, Wijesinghe KJ, Stahelin RV, Pang Y. Bright red-emitting highly reliable styryl probe with large Stokes shift for visualizing mitochondria in live cells under wash-free conditions. Sensor Actuator B Chem 2019;285:76–83.

[45] Möller A, Bleckenwegner P, Monkowius U, Mohr F. Gold(I)alkynyl complexes decorated with chromophores: structural, photophysical and computational studies. J Organomet Chem 2016;813:1–6.

[46] Pina J, de Melo JS, Breusov D, Scherf U. Donor–acceptor–donor thienyl/bithienyl-benzothiadiazole/quinoxaline model oligomers: experimental and theoretical studies. Phys Chem Chem Phys 2013;15:15204.

[47] Rietsch P, Sobottka S, Hoffmann K, Popov AA, Hildebrandt P, Sarkar B, Resch-Genger U, Eigler S. Between aromatic and Quinoid structure: a symmetrical UV to vis/NIR benzothiadiazole redox switch. Chem – A Eur J 2020;26:17361–5.

[48] Aguiló E, Moro AJ, Outis M, Pina J, Sarmento D, Seixas de Melo JS, Rodríguez L, Lima JC. Deactivation routes in gold(I) polypyridyl complexes: internal conversion Vs fast intersystem crossing. Inorg Chem 2018;57:13423–30.

[49] Ceriani C, Corsini F, Mattioli G, Mattiello S, Testa D, Po R, Botta C, Griffini G, Beverina L. Sustainable by design, large Stokes shift benzothiadiazole derivatives for efficient luminescent solar concentrators. J Mater Chem C 2021;9:14815–26.

[50] Reichardt C. Solvents and solvent effects in organic chemistry. Weinheim: Wiley-VCH; 2003.

[51] Mukhopadhyay A, Maka VK, Moorthy JN. Remarkable influence of 'phane effect' on the excited-state properties of cofacially oriented coumarins. Phys Chem Chem Phys 2017;19:4758–67.

[52] Pazini A, Maqueira L, Avila HC, Valente FM, Aderne RE, Back D, Aucélio RQ, Cremona M, Limberger J. Phenoxy-benzothiadiazole dyes: synthesis, photophysical properties and preliminary application in OLEDs. Tetrahedron Lett 2018;59: 2994–9.

[53] Gülseven Sidir Y, Sidir I. Solvent effect on the absorption and fluorescence spectra of 7-acetoxy-6-(2,3-dibromopropyl)-4,8-dimethylcoumarin: determination of ground and excited state dipole moments. Spectrochim Acta - Part A Mol Biomol Spectrosc 2013;102:286–96.

[54] Manning SJ, Bogen W, Kelly LA. Synthesis, characterization, and photophysical study of fluorescent N-substituted benzo[ghi]perylene "swallow tail" monoimides. J Org Chem 2011;76:6007–13.

[55] Rodríguez L, Ferrer M, Rossell O, Duarte FJS, Gil Santos A, Lima JC. Solvent effects on the absorption and emission of [Re(R$_2$bpy)(CO)$_3$X] complexes and their sensitivity to CO_2 in solution. J Photochem Photobiol A Chem 2009;204:174–82.

[56] Aliaga-Alcalde N, Rodríguez L. Solvatochromic studies of a novel Cd2+– anthracene-based curcuminoid and related complexes. Inorg Chim Acta 2012;380: 187–93.

[57] Zhang G-F, Aldred MP, Gong W-L, Li C, Zhu M-Q. Utilising tetraphenylethene as a dual activator for intramolecular charge transfer and aggregation induced emission. Chem Commun 2012;48:7711.

[58] de Aquino A, Caparrós FJ, Truong K-N, Rissanen K, Ferrer M, Jung Y, Choi H, Lima JC, Rodríguez L. Gold(I)-doped films: new routes for efficient room temperature phosphorescent materials. Dalton Trans 2021;50:3806–15.

[59] Caparrós FJ, Outis M, Jung Y, Choi H, Lima JC, Rodríguez L. Luminescent tetranuclear gold(I) dibenzo[g,p]chrysene derivatives: effect of the environment on photophysical properties. Molecules 2020;25:949.

[60] Sun Q, Aragay G, Pinto A, Aguiló E, Rodríguez L, Ballester P. Influence of the attachment of a gold(I) phosphine moiety at the upper Rim of a Calix[4]pyrrole on the binding of tetraalkylammonium chloride salts. Chem – A Eur J 2020;26: 3348–57.

[61] Frisch MJ, Schlegel HB, Scuseria GE, Robb MA, Cheeseman JR, Scalmani G, Barone V, Mennucci B, Petersson GA, Nakatsuji H, Caricato M, Li X, Hratchian HP, Izmaylov AF, Bloino J, Zheng G, Sonnenberg JL, Hada M, Ehara M, Toyota K, Fukuda R, Hasegawa J, Ishida M, Nakajima T, Honda Y, Kitao O, Nakai H, Vreven T, Montgomery JA, Peralta JE, Ogliaro F, Bearpark M, Heyd JJ, Brothers E, Kudin KN, Staroverov VN, Keith T, Kobayashi R, Normand J, Raghavachari K, Rendell A, Burant JC, Iyengar SS, Tomasi J, Cossi M, Rega N, Millam JM, Klene M, Knox JE, Cross JB, Bakken V, Adamo C, Jaramillo J, Gomperts R, Stratmann RE, Yazyev O, Austin AJ, Cammi R, Pomelli C, Ochterski JW, Martin RL, Morokuma K,

Zakrzewski VG, Voth GA, Salvador P, Dannenberg JJ, Dapprich S, Daniels AD, Farkas O, Foresman JB, Ortiz JV, Cioslowski J, Fox DJ. 1, mj frisch, gw trucks, hb schlegel, ge scuseria, ma robb, jr cheeseman, g. Scalmani, v. Barone, b. Mennucci, ga petersson et al. Gaussian 09 (Revission B.1); Gaussian Inc.: Wallingford CT Gaussian. Inc., Wallingford CT 2010;121:150–66. 2009.

[62] Becke A. Density-functional thermochemistry. III. The role of exact exchange. J Chem Phys 1993;98:5648–52.

[63] Lee C, Yang W, Parr RG. Development of the colle- salvetti correlation-energy formula into a functional of the electron density. Phys Rev B Condens Matter 1988; 37:785–9.

[64] Weigend F, Ahlrichs R. Balanced basis sets of split valence, triple zeta valence and quadruple zeta valence quality for H to Rn: design and assessment of accuracy. Phys Chem Chem Phys 2005;7:3297–305.

[65] Schäfer A, Horn H, Ahlrichs R. Fully optimized contracted Gaussian basis sets for atoms Li to Kr. J Chem Phys 1992;97:2571–7.

[66] Casida ME, Jamorski C, Casida KC, Salahub DR. Molecular excitation energies to high-lying bound states from time-dependent density-functional response theory: characterization and correction of the time-dependent local density approximation ionization threshold. J Chem Phys 1998;108:4439–49.